Bioresource Technology 247 (2018) 273–281

Contents lists available at ScienceDirect

Bioresource Technology

journal homepage: www.elsevier.com/locate/biortech

Pyrolysis of *Arundo donax L.* to produce pyrolytic vinegar and its effect on the growth of dinoflagellate *Karenia brevis*

Hao Zheng[a,b,1], Cuizhu Sun[a,b,1], Xiaodong Hou[c], Miao Wu[a,b], Yuan Yao[a,b], Fengmin Li[a,b,*]

[a] Institute of Coastal Environmental Pollution Control, Key Lab of Marine Environmental Science and Ecology, Ministry of Education, Ocean University of China, Qingdao 266100, China

[b] College of Environmental Science and Engineering, Ocean University of China, Qingdao 266100, China

[c] Institute of Geochemistry, Chinese Academy of Sciences, Guiyang 550081, China

GRAPHICAL ABSTRACT

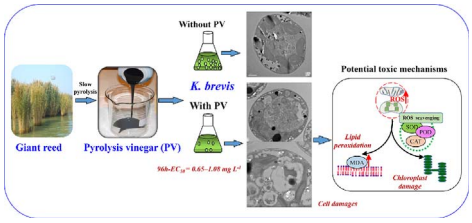

ARTICLE INFO

Keywords:
Wetland plant
Slow pyrolysis
Biomass valorization
Algaecide
Oxidative stress

ABSTRACT

Harmful algal blooms (HABs) have become global environmental issues, and the demand for alternative algaecides is urgent. Pyrolytic vinegars (PVs) were pyrolyzed from giant reed at 300–600 °C to investigate the underlying mechanisms of their inhibitory effect on the red tide dinoflagellate *Karenia brevis* by sub-chronic toxicity experiments. The major components of PVs were acetic acid, phenols, aldehyde, ketone, and esters. The 96 h median effective concentration (96 h-EC_{50}) values of PVs were 0.65–1.08 mL L^{-1}, and PV300 showed the strongest inhibitory effect. The increased contents of reactive oxygen species (ROS) and malondialdehyde, antioxidant enzymes activities indicated that *K. brevis* cells were suffering from oxidative stress, leading to lipid oxidation and cell structure damage. The sites of ROS accumulation in the treated cells were chloroplasts and mitochondria. These results suggest the suitability of PVs as potential algaecides for HAB control, and also provide a new direction for biomass valorization.

1. Introduction

Harmful algal blooms (HABs), involving explosive proliferation and accumulation of algae at extremely high cell densities (> 1000 cells mL^{-1}), have been increasing worldwide (Kudela and Gobler, 2012). These have resulted from global climate change and exacerbating eutrophication as a result of expanding human activities such as wastewater discharge, aquaculture, and fertilizer leaching (Chen et al., 2012; Mcfarland et al., 2016). The regions in which HABs occur are increasing annually. Approximately 107 places suffered from HABs worldwide in 2016, although they were only observed in 15 regions in 1970 (WHOI, 2016). China is one of the countries that have suffered from severe HABs. According to China's Marine Environment Quality Bulletin in 2016, the occurrence of red tide increased from 46 times (within 4070 km^2) in 2013–68 times (within 7484 km^2) in 2016. These blooms led to severe water quality deterioration and high fish

* Corresponding author at: Institute of Coastal Environmental Pollution Control, Key Lab of Marine Environmental Science and Ecology, Ministry of Education, Ocean University of China, Qingdao 266100, China
E-mail address: lifengmin@ouc.edu.cn (F. Li).
[1] These two authors contributed equally to this work.

http://dx.doi.org/10.1016/j.biortech.2017.09.049
Received 29 June 2017; Received in revised form 5 September 2017; Accepted 6 September 2017
Available online 08 September 2017
0960-8524/

mortality by a combination of reduced dissolved oxygen in the water and production of algal toxins. They were responsible for annual losses of about 726 million USD. *Karenia brevis* (*K. brevis)* is a single-celled planktonic organism called a dinoflagellate, and one of the harmful red tide species that occur worldwide in oceans (Fleming et al., 2011). During blooms, *K. brevis* may cause neurotoxic poisoning of marine organisms like fish and mollusks (Mcfarland et al., 2016). In consequence, the effective control of *K. brevis* HABs has become an urgent task for protection and exploitation of marine ecosystems.

Many strategies, including the use of chemical algaecides, physical adsorption, biological control, and mechanical collection of bloom biomass, have been applied to avoid and reduce the potential risks associated with HABs (Chen et al., 2012; Jančula and Maršálek, 2011). As an emergency measure, mechanical collection was effective and widely used in freshwater lakes such as Lake Taihu during bloom seasons in China (Chen et al., 2012). However, ecological risks to terrestrial plants (e.g., crops and wild grass) due to absorption and accumulation of microcystins (MCs), and risks to human health associated with consumption of MC-contaminated groundwater and crops occurred once the toxic bloom organisms and toxin-contaminated water were transferred to soil (Chen et al., 2006, 2012). One of the most promising physical strategies has been the use of suspended clay particles over the blooms to flocculate the planktonic cells, but the high clay load results in high mortalities among suspension-feeding bivalves like *Argopecten irradians* (bay scallop) and *Mytilus edulis* (blue mussel) (Archambault et al., 2004). The use of algaecides like ferric chloride, copper sulfate, and hydrogen peroxide is a quick and efficient approach, but these poisons may indiscriminately kill other organisms in the aquatic ecosystem and cause secondary pollution (Jančula and Maršálek, 2011). For instance, copper compounds (copper oxychloride, cuprous oxide, and copper sulfate), which have been intentionally introduced into water bodies as aquatic plant herbicides or algaecides, have been shown to result in water pollution owing to their elevated concentrations in the water (de Oliveira-Filho et al., 2004). Thus, eco-friendly algaecides that would act on only certain species instead of causing widespread mortality among organisms are urgently needed.

Pyrolysis is the thermal degradation of biomass under anoxic conditions, which may produce syngas, biochar or charcoal, and bio-oil (also called pyrolytic vinegar: PV) (Collard and Blin, 2014; Saikia et al., 2015). Biochar, as the main product of biomass pyrolysis, has been studied extensively in relation to carbon (C) sequestration (Zheng et al., 2018), soil improvement (Zheng et al., 2017), and alternative energy supply (Saikia et al., 2015). However, PVs are usually ignored during biochar production using slow pyrolysis technology (Rahmat et al., 2014). Even if PVs are recycled, researchers are mainly concerned with PV energy characteristics and values (Saikia et al., 2015). In addition to energy values, PVs are considered potentially valuable chemicals that could be utilized as bactericides (Yang et al., 2016), soil amendment (Lashari et al., 2015), and botanical protection (Rahmat et al., 2014) because of their high antimicrobial and antioxidant activity (Yang et al., 2016). In addition, the macrophyte allelochemicals such as polyphenols, esters, and alkaloids extracted from wetland plants (e.g., *Phragmites communis*, *Eichhornia crassipes*, *Stratiotes aloides*), of which the chemical compositions were similar to PVs (Temiz et al., 2013), were successfully used to control algal growth (Meng et al., 2015; Gao et al., 2017). Therefore, it is reasonable to hypothesize that the PVs may have similar anti-algal effect and may be potential algaecides useful for HAB control.

Therefore, the specific objectives of this study were to: 1) characterize the physico-chemical properties of the PVs formed by pyrolysis of giant reed (*Arundo donax L.*) at 300–600 °C, 2) investigate the effects of these PVs on *K. brevis* growth, and 3) illustrate the potential underlying mechanisms responsible for the inhibited growth of *K. brevis*. These findings will provide information useful for producing PV-derived alternative algaecide for HAB control, and will also provide a new way of biomass valorization.

2. Materials and methods

2.1. Preparation and characterization of PVs

Giant reed is a common wetland plant that is widely applied in water purification and ecological restoration in China owing to its rapid rate of growth and good resistance to drought and floods (Zheng et al., 2013). The reeds used to produce the PV in this study were collected from Nansi Lake wetland (37° 24′ 43″ N, 118° 39′ 49″ E) in August. The reed shoots were cut into small pieces (1 × 3 cm), and dried at 80 °C for 24 h. The PV was produced using slow pyrolysis as described by Zheng et al. (2013). In brief, 50 g of giant reed stems were pyrolyzed at 300, 400, 500, or 600 °C for 4 h using a vacuum-quartz-tube furnace (GSL-1300, MTI, China) under a N_2 flow of 200 mL min^{-1}. The PV samples were collected via a condenser filled with an ice-water mixture, and then filtered through a 0.45 μm cellulose acetate membrane. The corresponding treatments are hereafter referred to as PV300, PV400, PV500, and PV600, respectively. The yields of PV and biochar were recorded and all the PV samples were kept at 4 °C in the dark for further analysis.

The density of the PV was measured using an optical density meter (LS117, Linshang, China). Moisture content was measured using Karl Fischer volumetric titration with a moisture analyzer (870 KF Titrino plus, Metrohm, Switzerland). The chemical composition of the PV was determined using an Agilent Gas Chromatography-Mass Spectrometer (GC–MS, 7890A-5957C, Agilent, USA). The GC–MS analysis was carried out with the following oven temperature programming (Yang et al., 2016): initial temperature 50 °C for 2 min, ramped at 15 °C min^{-1} to 250 °C; then held at 250 °C for 5 min. One microliter of PV sample was injected into the column with a split ratio of 20:1, and the electron impact mass spectrum was obtained at 70 eV. The relative contents of the compounds were determined by the corresponding peak areas (Wu et al., 2015).

2.2. Exposure of K. brevis to PVs

The *K. brevis* tested were obtained from the Institute of Oceanology, Chinese Academy of Science. The algae were cultivated in 200 mL f/2 medium. The culture vessels were 500 mL Erlenmeyer flasks, which were autoclaved (121 °C) for 20 min before inoculation. The algae were cultivated under a light/dark cycle of 14:10 h at 23 ± 1 °C with 4000 lux illumination in an intelligent artificial climate box (GXZ-380Z, Jiangnan, China). Every flask was gently shaken by hand three times every day.

For all the experiments, 200 mL of *K. brevis* was taken from the stock culture at log phase of growth (1.2×10^5 cells mL^{-1}) and added to 500 mL Erlenmeyer flasks under sterile conditions. PV portions of (0, 40, 80, 120, 16, and 200) μL were diluted in 200 mL portions of *K. brevis* solution to reach the desired concentrations of (0, 0.2, 0.4, 0.6, 0.8, and 1.0) mL L^{-1}, respectively. The treatments are hereafter referred to as CK, PV-0.2, PV-0.4, PV-0.6, PV-0.8, and PV-1.0, respectively. Each treatment was replicated three times. The algae were sampled and the densities were counted using a hemocytometer with a Nikon microscope (E100-LEO, Nikon, Japan) every 24 h for 7 d. The inhibitory ratio (*IR*, %) of *K. brevis* upon PV exposure was calculated using the following equation:

$$IR\,(\%) = (1 - N/N_0) \times 100 \quad (1)$$

where N and N_0 is the number of algae in the PV and CK treatments at the specific sampling time, respectively. Additionally, the morphology of K. brevis cells were determined by a transmission electron microscope (TEM, JEOL-JEM-1200EX, Japan) (Li et al., 2015).

2.3. Estimation of malondialdehyde (MDA) and oxidative stress

To measure the MDA content and antioxidant enzyme activities

(including superoxide dismutase: SOD, catalase: CAT, and peroxidase: POD) of *K. brevis*, 20 mL algal solution was sampled at (0, 24, 48, and 72) h, respectively, and centrifuged at 3000 r min^{-1} for 15 min. Then the alga pellets were re-suspended in 2 mL PBS (0.05 M, pH 7.8), and sonicated (KS-500F, Ningbo, China) at 4 °C for 5 min. Subsequently, the MDA content, and the SOD and CAT activity, were measured in accordance with the manufacturer instructions in the commercial assay kits (Jiancheng, Nanjing, China) (Li et al., 2015).

The content of reactive oxygen species (ROS) was determined using oxidation sensitive probes with the dichlorofluorescein diacetate (DCFH–DA) method (Gu et al., 2017). Briefly, 1 mL of alga solution was centrifuged at 3000 r min^{-1} for 10 min, and the solid residue was re-suspended in a mixture of 1 mL of 10 mM oxammonium hydrochloride and 1 mL 10 mM DCFH-DA solution. This was incubated in the dark at 25 °C on a rocking shaker (ZQTY-50, Zhichu, China) for 20 min. Then the fluorescence intensity of the supernatant was measured using a fluorescence spectrophotometer (F-4600, Hitachi, Japan) at 530 nm to represent the ROS production. The contents of superoxide anion (O_2^-), $^{\cdot}OH$ and H_2O_2 were detected using a UV-vis spectrophotometer (UV-2550, Shimadzu, Japan) at 405, 550, and 405 nm, respectively (Li et al., 2015).

2.4. Electron transport chain inhibitors to the algae

To distinguish the sites of ROS production and accumulation in the algal cells, diuron, rotenone, and dicumarol were used as the electron transport chain (ETC) inhibitors of chloroplast, mitochondrion, and plasmalemma, respectively (Van et al., 2016). Diuron can bind with the secondary quinone acceptor (QB) protein and inhibit plastoquinone (PQ) reduction in chloroplasts, thereby blocking electron transfer from the primary quinone acceptor (QA) to QB in chloroplast ETC (Laisk and Oja, 2013). Rotenone can inhibit electron transfer from nicotinamide adenine dinucleotide (NADH) to ubiquinone (CoQ, complex I) in mitochondrion, resulting in ROS generation in sub-mitochondrial particles (Van et al., 2016). Moreover, the test concentrations of these chemicals were pre-tested to ensure that they were harmless to algal growth. Three groups of the algae were cultivated in the f/2 medium for 30 min, wherein the concentrations of rotenone, diuron, and dicumarol were (5, 1.25, and 5) μg L^{-1}, respectively; then they were each treated with 100 μL PV300 to make sure the final concentration of PV300 was 0.5 mL L^{-1}. Another four groups of the algae were cultivated in the f/2 medium, wherein the concentrations of rotenone, diuron, dicumarol, and PV300 were (5, 1.25, 5) μg L^{-1}, and 0.5 mL L^{-1}, respectively. One group of algae without any treatment was also cultivated as control. All these groups of algae were cultivated for 24 h. Afterwards, the ROS production in the algae was measured using the same method as mentioned above.

2.5. Statistical analysis

Results are expressed as the mean values of three replicates with standard deviation. Different small letters in the figures and tables indicate the significance of the various parameters among different PV treatments, which was tested using one-way analysis of variance (ANOVA) by Tukey's test by means of Statistical Product and Service Solutions Software 20.0 (SPSS 20.0). The correlation was analyzed using Pearson test (two-tailed) at $P < 0.05$ by means of SPSS 20.0.

3. Results and discussion

3.1. Effects of pyrolytic temperature on PV properties

The properties of the PV are presented in Table 1. With increasing pyrolysis temperature from 300 to 600 °C, the mass yield of PV significantly increased from 19.2 to 20.9% ($r = 0.999$, $P < 0.05$), whereas the biochar mass yield significantly decreased from 43.6 to 29.0% ($r = -0.989$, $P < 0.05$). These results indicated that more volatile matter was emitted, but less biochar was produced from the reeds as the pyrolytic temperature rose in the range 300–600 °C. The lower yield of PV (compared to other studies) is attributed to the slower heating rate of 10 °C min^{-1} and lower cooling efficiency of the self-designed condenser (Demiral and Ayan, 2011). Furthermore, the higher yield of PV at higher temperature (e.g., 600 °C) resulted from the more vigorous decomposition of abundant cellulose and lignin contained in the giant reed (Wu et al., 2015), of which the content was 45.1% and 22.4%, respectively (Temiz et al., 2013). In addition, the moisture content increased from 61.2 to 67.0% with increasing pyrolysis temperature ($r = 0.999$, $P < 0.05$) because of the original moisture in the feedstock and biomass dehydration during pyrolysis (Demiral and Ayan, 2011). Regardless of the pyrolytic temperature, the PV density remained stable at 1.00–1.04 g mL^{-1}, similar to the density of 1.02 g mL^{-1} in wood vinegar from teak-wood waste (Rahmat et al., 2014). The pH values decreased non-significantly from 3.07 for PV300 to 2.74 for PV600, showing the acidic feature was due to predominantly acidic chemicals (e.g., acetic acid) in the PVs (Table 2).

Table 1
The selected physico-chemical properties of the PVs produced from giant reed at different temperatures.

PVs[a]	Yield (%)	pH	Density (g mL^{-1})	Moisture content (%)	Biochar yield (%)
PV300	19.2a[b]	3.07a	1.03a	61.2a	43.6c
PV400	19.7b	2.74a	1.00a	63.4b	34.1b
PV500	20.1c	2.78a	1.05a	65.2c	32.1ab
PV600	20.9d	2.77a	1.03a	67.0d	29.0a

[a] PV300–600 indicate that the pyrolytic vinegar (PV) produced at 300–600 °C.
[b] Different small letters behind the data within same column indicate significant difference among the different PVs, which was analyzed by SPSS 20.0 ($P < 0.05$).

A total of 25 chemical compounds were identified, representing 82.8–88.8% of the composition of the PV (Table 2). The major components of the PV were acetic acid, phenols, aldehyde, ketone, alcohol, and esters, totally accounting for 78.8–81.9% of the PVs. The relative content of the total organic acid and aldehyde in the PV significantly decreased from 56.5% and 5.13% at 300 °C to 47.7% and 3.68% at 600 °C, respectively, whereas the relative content of ketone significantly increased from 7.90% at 300 °C to 11.1% at 600 °C (Table 1). Similarly, the relative content of the representative components (e.g., acetic acid, furfural, guaiacol) also exhibited decreasing trends with the increasing pyrolytic temperature from 300 to 600 °C. The changes of these chemical components were attributed to the degree of decomposition of hemicellulose, cellulose, and lignin contained in the feedstock at the different pyrolysis temperatures (Collard and Blin, 2014; Demiral and Ayan, 2011). Specifically, the hemicellulose started to decompose at 100–260 °C, then was followed by the destruction of cellulose at 240–350 °C and lignin at 280–500 °C (Liu et al., 2017). The higher content of acetic acid at lower temperature (e.g., 300 °C) relative to higher temperature (e.g., 600 °C) was ascribed to the breakage of the acetyl groups in the hemicelluloses and celluloses (Liu et al., 2017), but this thermally unstable product might be susceptible to decomposition at a higher temperature, resulting in a lower yield at a higher temperature (Wang et al., 2009). The higher content of phenols (12.7–13.7%) in the higher temperature PV (e.g., PV500) was attributed to the more vigorous decomposition of lignin, with cross-linked structures of various hydroxyl- and methoxy-substituted phenylpropane units occurring at higher temperature (Wu et al., 2015). Consistently, Wu et al. (2015) found that the maximum weight loss of lignin degradation was around 450 °C. Moreover, Brebu et al. (2013) also highlighted that the maximum rate of lignin degradation was at 370–385 °C, and the mass loss slowly continued above 550 °C.

It has been reported that certain components in algaecides such as benzoic acid, phenolics, and furfural could significantly inhibit the

Table 2
Main components of the PV produced from giant reed at different temperatures.

Number	Category	Compounds	Retention time (min)	Relative content (%)[a]			
				PV300[b]	PV400	PV500	PV600
1	Organic acid	Acetic acid	7.88	49.5	45.6	42.4	40.0
2		Propanoic acid	8.80	2.03	2.26	2.26	2.01
3		Benzoic acid	9.55			1.77	
		Total[c]		51.5	47.9	46.4	42.0
4	Phenol	2,6-dimethoxyphenol	14.0	4.96	5.20	6.07	5.70
5		Guaiacol	11.4	3.15	3.09	3.04	2.91
6		2-methoxy-4-vinylphenol4	13.6	1.07	1.11	0.99	0.88
7		Phenol	12.4	1.04	1.46	1.91	1.76
8		Desaspidinol	19.7	1.24		1.72	1.42
		Total		11.5	10.9	13.7	12.7
9	Aldehyde	Furfural	8.17	3.65	2.77	2.29	2.16
10		5-hydroxymethylfurfural	15.4	1.48	1.56	1.83	1.52
		Total		5.13	4.33	4.12	3.68
11	Ketone	hydroxyacetone	6.64	3.36	5.48	5.47	5.57
12		acetonyl acetate	8.11	2.13	1.92	1.72	1.70
13		1-Hydroxy-2-butanone	7.35	1.24	1.88	1.74	1.86
14		2-hydroxy-3-methylcyclopent-2-enone	11.1	1.07	1.41	1.94	1.94
		Total		7.80	10.7	10.9	11.1
15	Alcohol	2-Furanmethanol	9.79	2.39	2.70	2.29	2.77
16		Tetrahydrofurfuryl alcohol	8.56				4.04
17		Homovanillyl alcohol	16.4	0.88	0.91	1.29	1.09
		Total		3.27	3.61	3.58	7.90
18	Esters	2(3H)-Furanone, dihydro-4-hydroxy	13.1	2.87	3.01		
19		Butyrolactone	9.69	1.08	1.41	1.54	1.45
		Total		3.95	4.42	1.54	1.45
20	Others	N-Methyl-1,3-propanediamine	6.43			4.02	3.66
21		2,3-Dihydrobenzofuran	14.8	1.90	1.92	1.39	1.43
22		1,2,4-Trimethoxybenzene	14.5	1.45	1.62		1.59
23		Butane, 2,2-dimethyl				1.10	
24		4-Ethylbiphenyl	13.5			1.10	
25		Isobutyric anhydride	8.56		0.96	0.95	1.31
		Total		3.35	0.96	8.56	7.99

[a] The relative contents of the compounds were determined by the corresponding peak areas (Wu et al., 2015).
[b] PV300–600 indicates the pyrolytic vinegars (PVs) produced at 300–600 °C.
[c] "Total" indicates the total relative content of the compounds in each category.

growth of algae (e.g., *Microcystis flos-aquae, Chlamydomonas reinhardtii)* (Guo et al., 2015; Liang et al., 2013). Accordingly, it was assumed that PV, which contains organic acid, phenol, and aldehyde, might also have the same anti-algal effect as algaecides. In addition, in view of the different ratio and content of the major components (i.e., organic acid, phenol) in PV produced at 300–600 °C, there might exist varying degrees of inhibitory effect on *K. brevis* growth by PV produced under different conditions. Therefore, the following experiments were designed to screen the PVs produced at certain temperatures for their strongest inhibitory effect on *K. brevis*.

3.2. Inhibitory effect of PV on K. brevis

The effect of PVs produced at 300–600 °C on the *K. brevis* growth is shown in Fig. 1. For the PV300 treatments, the algal densities significantly decreased by (6.1, 17.3, 48.6, 64.2, and 78.8) % in the PV-0.2, PV-0.4, PV-0.6, PV-0.8, and PV-1.0 treatments, respectively, compared with CK at Day 7 (Fig. 1a). Similarly, PV400, PV500, and PV600 also showed inhibitory effects on algal growth (Fig. 1b–d). Moreover, the inhibitory ratios were (78.8, 64.7, 63.3, and 55.9) % for PV300, PV400, PV500, and PV600, respectively, in the PV-1.0 treatments at Day 7, and the 96 h median effective concentration values (96h-EC_{50}) were (0.65, 1.09, 1.04, and 1.08) mL L^{-1}, respectively. These results indicated that the PV300 with the 96h-EC_{50} of 0.65 mL L^{-1} had the highest inhibitory effect on the growth of *K. brevis*. This probably resulted from the higher content of furfural, acetol, and phenolics in PV300 (Table 2). Coincidentally, Liang et al. (2013) stated that the softwood-derived bio-oil fraction containing furfural, acetol, and phenolics significantly inhibited *Chlamydomonas reinhardtii* growth; but that acetic acid, formic acid, and methanol had no inhibitory effect. In addition, PV was more efficient at inhibiting algal growth when compared with allelochemicals including *cis*-6-octadecenoic and *cis*-9-octadecenoic, for which the reported 96h-EC_{50} was 1.6 and 3.3 mg L^{-1}, respectively (Nakai et al., 2005; Hong et al., 2009). These results confirmed that PV could serve as a potential alternative to the algaecides.

In addition, the effect of PVs on the cell viability of *K. brevis* at the end of the cultivation was also examined. For the PV300 treatments, the number of mobile *K. brevis* cells significantly decreased by (66.7, 68.6, 91.8, 100, and 100) % in the PV-0.2, PV-0.4, PV-0.6, PV-0.8, and PV-1.0 treatments, respectively, relative to CK treatment at Day 7. The good negative correlations between the PV300 concentrations and the mobile cells ($r = -0.879$, $P < 0.05$) confirmed the dosage-dependent toxicity effect of PV300 on algal growth. To a certain degree, the mortality rate of algae is closely related to the cell viability because the immobile algae could coagulate and sink to the water bottom, then their growth would be inhibited due to the lack of sufficient light (Zhou et al., 2008). Furthermore, PV400, PV500, and PV600 showed similar effects on algal viability. Moreover, the inhibitory ratios were 91.8, 76.9, 68.6, and 49.4% for PV300, PV400, PV500, and PV600, respectively, in the PV-0.6 treatments at Day 7. It turned out that the PV exposure significantly inhibited the cell viability of *K. brevis* and that the inhibitory effect of PV300 was the strongest. This was in line with the result that PV300 has the strongest inhibitory effect on algal growth, as was confirmed by the good correlation between the immobilized cells and the algal densities

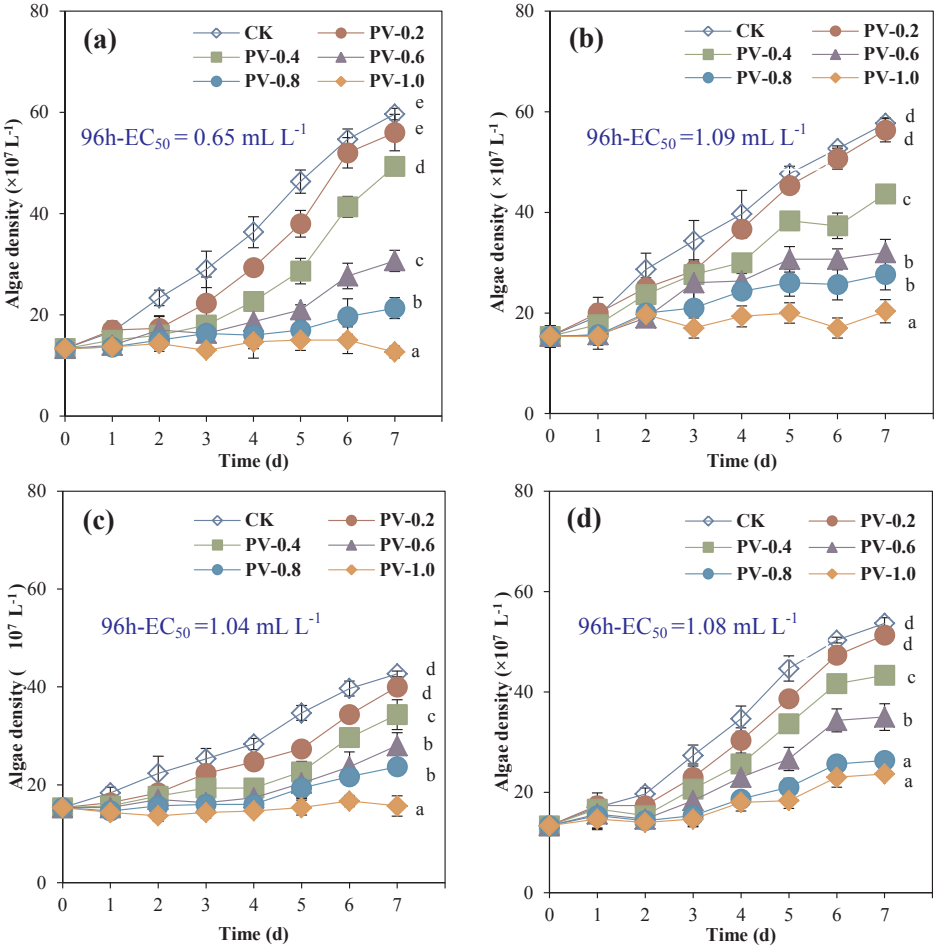

Fig. 1. The growth curves of *K. brevis* exposed with the PVs produced at different temperatures. (a) PV300; (b) PV400; (c) PV500; and (d) PV600. CK, PV-0.2, PV-0.4, PV-0.6, PV-0.8, and PV-1.0 indicate that the algae were treated with the PVs at the concentrations of 0, 0.2, 0.4, 0.6, 0.8, and 1.0 mL L^{-1}, respectively. Different small letters represent significant differences among the different concentrations of PV treatments, which were analyzed by SPSS 20.0 ($P < 0.05$). The error bars represents standard deviation ($n = 3$).

($r = 0.981$, $P < 0.05$). Therefore, the PV300 was chosen as the test alternative algaecide to further investigate the underlying mechanisms.

3.3. Effects of pH changes induced by PVs on K. brevis

The addition of PV to the algal culture medium may decrease its pH from 9.8 to 9.5–6.7 with increasing PV concentrations from 0.2 to 1.0 mL L^{-1} (Fig. 2a), because of the inherent acidity of the PV (Tables 1–2). To confirm whether the inhibitory effect of PVs was caused by the change in pH of the culture medium, the pH of the culture medium and the algal density at different initial pH (4–8) was determined (Fig. 2b–c). After seven days, the culture medium pH was not significantly different among the treatments at pH-6, pH-7, pH-8, and CK; whereas the pH-4 and pH-5 treatments significantly decreased the culture pH from 9.8 in CK, to 4.08 and 5.68, respectively. There was no consistent significant difference in the algal density observed between the treatments at pH-6, pH-7, pH-8, and CK, but the alga density significantly decreased after treatments of pH-4 and pH-5, with respect to the CK. These results implied that the pH change in the culture medium induced by the acidic PVs was not responsible for the inhibited algal growth. Similarly, the growth rate of *Skeletonema costatum* was nearly constant in medium containing 4 mL L^{-1} acetic acid due to its relatively low concentration (Liang et al., 2013). In photoautotrophic cultures, the increased uptake rate of inorganic carbon by algae at pH < 8.3 could result in a decrease of CO_2 partial pressure and thus lead to an increase in pH of the culture medium (Juneja et al., 2013). In addition, acid-tolerant algae (e.g., *Chlorella saccharophila*, *Euglena mutabilis*) can change their intracellular pH in response to the changed external pH, thus the algal growth would not be drastically affected by acidic conditions (Juneja et al., 2013). However, at extremely low pH (e.g., 1.4–3.4), the algal growth could be inhibited due to increased content of saturated fatty acid in the algal cell membrane, which may reduce membrane fluidity (Poerschmannet al., 2004). For example, the growth of *Chlamydomonas sp.* was significantly inhibited at pH 2.7 (compared with pH 7) due to the total fatty acid content increase from 2% at pH 7 to 2.4% at pH 2.7 (Poerschmannet al., 2004). Therefore, in view of the lack of inhibitory effect on algal growth by acetic acid addition in the treatments pH-6, pH-7, pH-8, and CK, it is reasonable that the acetic acid contained in PV was not responsible for the inhibition of *K. brevis*. In addition, considering the inhibitory effects of benzoic acid, phenolics, acetol, and furfural on microalgae like *Microcystis flos-aquae* and *Chlamydomonas reinhardtii*, the inhibitory effect may result from these components in our PV (Guo et al., 2015; Liang et al., 2013). The potential underlying mechanisms might be related to organelle damage, ROS proliferation, or lipid peroxidation caused by these compounds in the PV (Gao et al., 2017; Hong et al., 2009), which will be discussed in the following sections.

3.4. Effects of PVs on algal cell ultrastructure

Inhibition of algal growth could be induced by damage to algal cell structures such as cell membranes and organelles, which was addressed by study of the ultrastructure of *K. brevis*. Although the cells treated with PV300 at 0.5 mL L^{-1} were intact, the borders of the mitochondria, chloroplasts, and nucleus were obscure. The lamellar structure of the chloroplasts was destroyed and the mitochondrion had disintegrated. Obvious and massive cell vacuolization appeared in the PV300 treated cells. Moreover, for the cells treated with the higher concentration of PV300 (PV-1.0), the plasma membrane had ruptured and all organelles had disintegrated, leaving only cell debris. This is consistent with

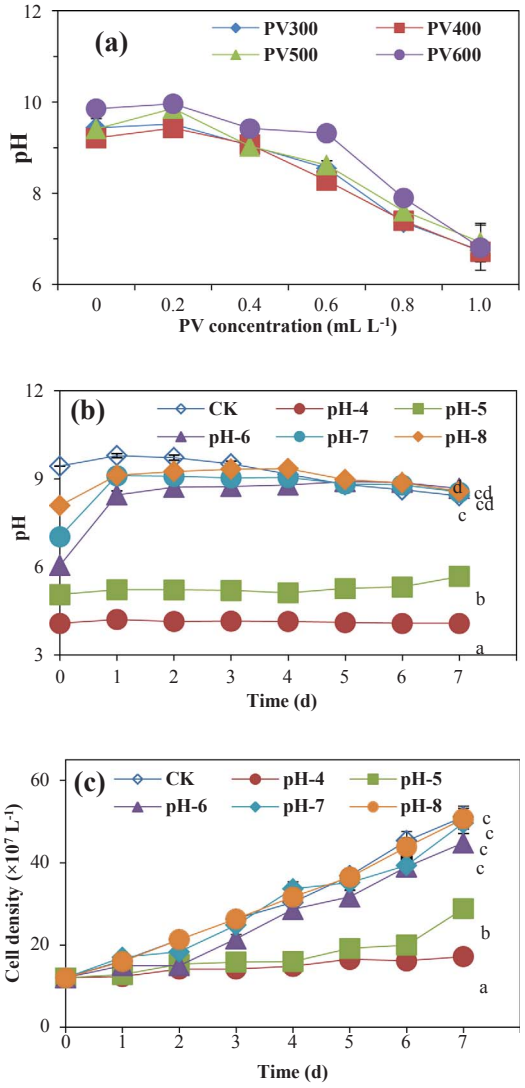

Fig. 2. The pH values of *K. brevis* culture treated with PVs (a) and acetic acid (b); effects of different pH on algal cell density (c). pH-4, pH-5, pH-6, pH-7, and pH-8 indicate that the initial pH of alga cultures treated with acetic acid are 4, 5, 6, 7 and 8, respectively. CK indicate that the initial pH of the culture is 9.8, which is not adjusted before cultivation. Different small letters represent significant differences among the different concentrations of PV treatments, which were analyzed by SPSS 20.0 ($P < 0.05$). The error bars represent standard deviation ($n = 3$).

concentration-dependent toxicity of PV to the algae density (Fig. 1). Hence, the algal cell structural damage signified efficient inhibitory effect of PV300 on the growth of *K. brevis*. Given the damage to the plasma membrane and organelles, including mitochondria and chloroplasts, a series of physiological and biochemical reactions such as photosynthesis and respiration would be interrupted, even causing oxidative stress (Li et al., 2015).

3.5. Oxidative stress of K. brevis caused by PV

The production and accumulation of ROS in the target cells, an indicator of oxidative stress, is frequently used to assess contaminant toxicity to organisms (Gu et al., 2017; Felix et al., 2017). The impacts of PV300 on the contents of ROS, $^{\cdot}OH$, O_2^-, and H_2O_2 in *K. brevis* are shown in Fig. 3. The ROS content was highly dependent on the PV300 concentration and cultivation time (Fig. 3a). The ROS level in the PV-0.5 and PV-1.0 treatment at the end of cultivation (72 h) significantly increased by 1.27 and 2.01 times compared with that of CK, respectively; while it had little effect in the PV-0.2 treatment. Consistently, the content of $^{\cdot}OH$, O_2^-, and H_2O_2 exhibited trends similar to ROS production (Fig. 3b–d). However, the O_2^- content in the PV-0.5 treatment significantly decreased relative to CK at 48 h. These results indicated that PV300 exposure triggered ROS over-production in the algal cells by disrupting the equilibrium between ROS generation and scavenging (Sharma et al., 2012; Gu et al., 2017). In photosynthetic algal species, ROS are continuously produced as byproducts of various metabolic pathways, which mainly derive from the ETC in chloroplasts, mitochondria, and the plasma membrane (Li et al., 2015). Accordingly, the accumulation of ROS during the PV300 treatments could be attributed to the destruction of cell membrane, chloroplasts, and mitochondria, in which electronic transmission is disrupted, causing more electron leaks and subsequently producing higher levels of ROS (Li et al., 2015). Similarly, the significant increase of ROS was also observed in algae such as *Microcystis aeruginosa, Phaeodactylum tricornutum,* and *Pseudokirchneriella subcapitata* upon exposure to algaecides such as N, N-dimethyl-3-amino-methylindole (gramine), ethyl 2-methyl acetoacetate, and pyrogallic acid, proving that the oxidative stress was caused by these algaecides (Hong et al., 2009; Yang et al., 2011; Wang et al., 2011).

To reduce or eliminate the excess ROS, antioxidant enzymes including SOD, CAT, and POD, involved in the most basic defensive systems in cells, are stimulated to balance the ROS generation and scavenging (Felix et al., 2017; Gu et al., 2017). As shown in the Fig. 4, the SOD activity significantly increased by 3.3, 5.3, and 14.2 times in the PV-0.2, PV-0.5 and PV-1.0 treatments, respectively, compared with CK at 24 h (Fig. 4a). This implies that SOD was stimulated by PV300 exposure to balance the ROS proliferation. In addition, the SOD activity peaked at 24 h and then sharply declined in the PV-0.2 and PV-1.0 treatments, while the PV-0.5 treatment showed a trend of increase during the entire period of cultivation. The SOD activity initially increased under PV-0.2 exposure, then was followed by a decreasing trend due to the clearance of a small amount of excess ROS by SOD (Felix et al., 2017). However, when the cells were treated with PV-1.0, the system of ROS production and scavenging became severely imbalanced, resulting in excessive ROS accumulation, and eventually causing inhibition of the antioxidant system (Kwok et al., 2012). This was indicated by the sharp decline of SOD activity (Fig. 4a). Consistently, the activities of CAT and POD showed trends similar to that of SOD (Fig. 4b–c), but there was no significant increase in the PV-0.2 treatment relative to CK during 24–72 h. This was because the excessive O_2^- produced in the PV-0.2 treatment was eliminated in advance by SOD, the first line of resistance against ROS, avoiding further cell damage (Felix et al., 2017).

As ROS dramatically accumulates, lipid peroxidation in the cell membrane and organelle membranes may occur consequently, which could worsen cell damage (Liu et al., 2016). This was confirmed by the significant increase of MDA content at the higher concentration PV300 treatments (PV-0.5, PV-1.0) (Fig. 4d) and the positive correlation between MDA and ROS levels ($r = 0.965$, $P < 0.05$). At the end of cultivation, the MDA content in the PV-0.2, PV-0.5, and PV-1.0 treatments increased by 0.01, 1.60 and 4.38 times, respectively, relative to CK (Fig. 4d). These results suggested that the increased MDA content was attributable to the oxidation stress response induced by excessive ROS generation after PV300 exposure (Liu et al., 2016). Guo et al. (2015) reported that the increased MDA content in *Microcystis flos-aquae* induced by gallic acid was due to excess ROS accumulation resulting from oxidative stress. Overall, the increased content of ROS and MDA, and activities of the antioxidant enzyme, indicated that the cell of *K. brevis* suffered serious oxidative stress caused by excessive ROS production and accumulation, leading to lipid oxidation and growth inhibition.

3.6. ROS production sites in K. brevis upon exposure to PV

To determine in more detail the ROS production sites in the algal cells, the effects of rotenone, diuron, and dicoumarol on ROS content

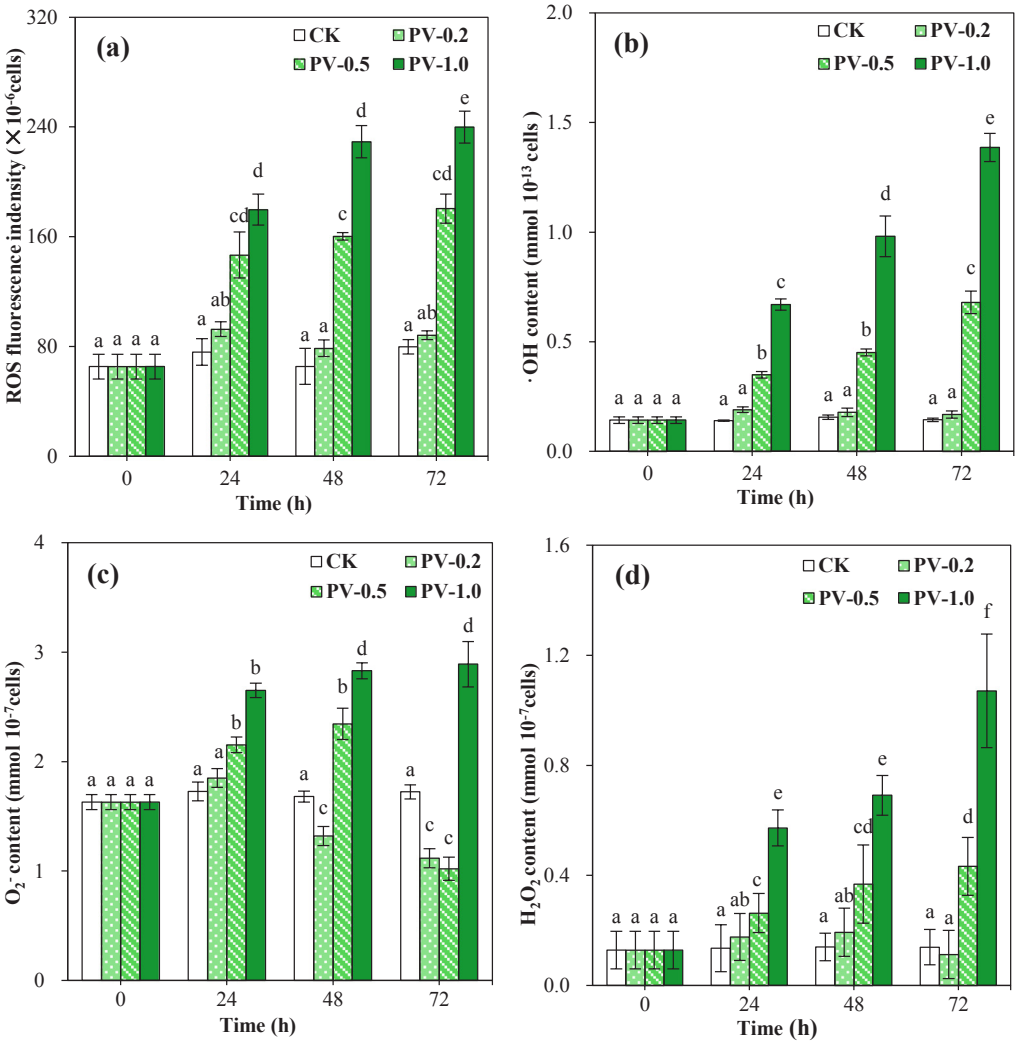

Fig. 3. Oxidative responses of *K. brevis* exposed with PV300. (a) ROS content; (b) ·OH content; (c) O_2^- content; and (d) H_2O_2 content. CK, PV-0.2, PV-0.5, and PV-1.0 indicate that the algae were exposed with the PV300 at the concentrations of 0, 0.2, 0.5, and 1.0 mL L^{-1}, respectively. Different small letters above the columns represent significant differences among the different concentrations of PV300 treatments at the same time, which were analyzed by SPSS 20.0 ($P < 0.05$). The error bars represent standard deviation ($n = 3$).

induced by PV300 were studied (Fig. 5). Compared to the PV300 treatment, the ROS production in the PV300 + Diu and PV300 + Rot treatments significantly decreased, indicating that the addition of diuron and rotenone could remove excess ROS caused by PV300, or that ROS produced by PV300 was inhibited, sequentially reducing the damage by PV300 to *K. brevis*. Given that diuron and rotenone are inhibitors of chloroplast and mitochondrial ETC, ROS produced by PV300 were found on the chloroplast and mitochondrial ETC. Thus, the action sites of PV300 on *K. brevis* cells were chloroplasts and mitochondria. Similar results were also reported by Li et al. (2015), who suggested that diuron could remove excess ROS produced by nano-TiO_2. Liu et al. (2016) also found that rotenone could significantly decrease the ROS content caused by dibutyl phthalate. However, the ROS production in the PV300 + Dic treatment had no significant difference relative to that of PV300 treatment, demonstrating that the addition of dicoumarol could not reduce the ROS generation caused by PV300, indicating that the plasma membrane was not the site for ROS accumulation. However, Liu et al. (2007) found that ROS accumulated in the plasma membrane of *Chattonella marina* under iron limitation because ferric reduction by plasma membrane ferric reductase was much greater than the iron uptake rate in *Chattonella marina*, and aerobic oxidation of excess Fe(II) could lead to ROS production. Furthermore, the degree of mitochondrial depolarization positively correlated with the PV300 concentrations ($r = 0.967$, $P < 0.05$), further confirming that PV300 targeted mitochondria. Meanwhile, the ·OH content in the isolated chloroplasts significantly increased from 15.0 U mL^{-1} in the CK treatment to 17.5 and 21.4 U mL^{-1} in the PV-0.2 and PV-0.5 treatments, respectively, verifying that the chloroplasts was also a site of ROS production induced by PV300 in *K. brevis*.

Overall, the potential toxicity mechanisms of PVs on *K. brevis* include the following aspects: 1) excess ROS was produced in the mitochondria and chloroplasts caused by PV exposure; 2) the lipid peroxidation that occurred in the cell membranes and organelles (e.g., mitochondria and chloroplasts) was attributable to the polyunsaturated fatty acid attacked by ROS; 3) damage to the internal cell structures (chloroplasts, mitochondria, and nucleus) was due to ROS accumulation in the cells. Although PV is considered an alternative algaecide against HABs, more studies are still needed before their practical application in control of HABs. Moreover, the environmental risk of PV to co-occurring species should be carefully considered. In addition, it is necessary to develop effective techniques to upgrade and separate specific active components such as benzoic acid, phenolics, and furfural in the complex PVs (Guo et al., 2015; Liang et al., 2013).

4. Conclusions

The major components of the PVs were acetic acid, phenols, aldehyde, ketone, alcohol, and esters. PV300 had the strongest inhibitory effect on *K. brevis* growth. The initial change of pH caused by acetic acid in PVs was not the reason for inhibition of *K. brevis*. The cell membranes and organelles were damaged and cell vacuolization became apparent in the PV treated alga cells, resulting from oxidative stress caused by

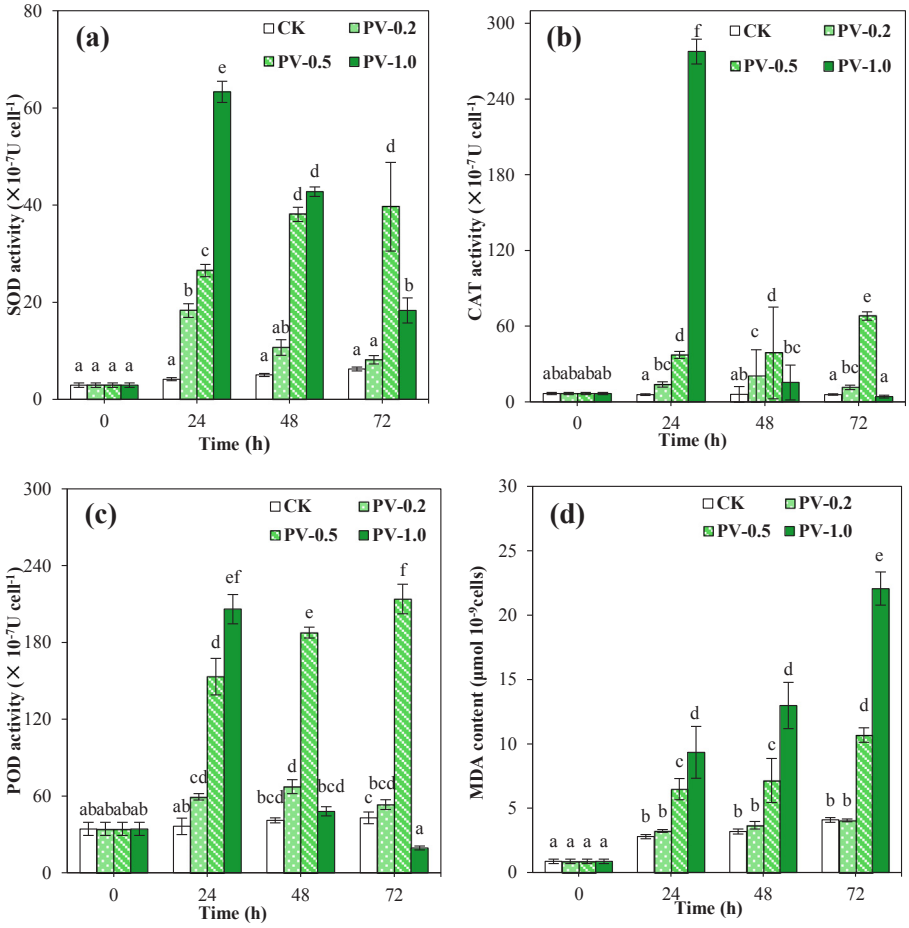

Fig. 4. Antioxidant enzyme activities of *K. brevis* exposed with PV300. (a) SOD; (b) CAT; (c) POD; and (d) MDA content. CK, PV-0.2, PV-0.5, and PV-1.0 indicate that the algae were exposed with the PV300 at the concentrations of 0, 0.2, 0.5, and 1.0 mL L^{-1}, respectively. Different small letters above the columns represent significant differences among the different concentrations of PV300 treatments at the same time, which were analyzed by SPSS 20.0 ($P < 0.05$). The error bars represent standard deviation ($n = 3$).

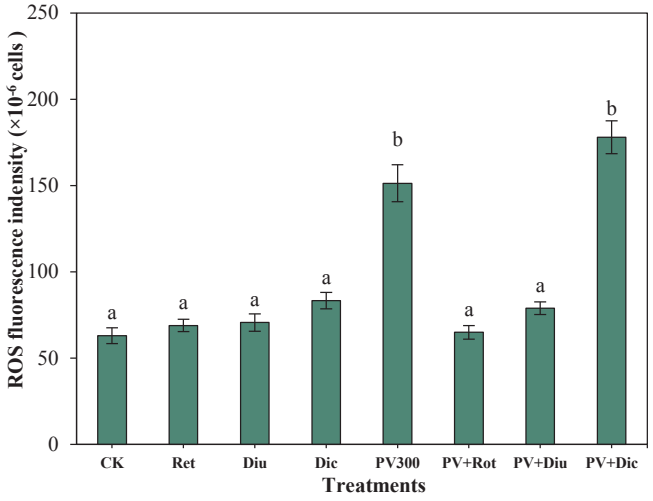

Fig. 5. Effects of the selected electron transfer inhibitors on ROS production of *K. brevis*. PV300: the pyrolytic vinegar (PV) produced from giant reed at 300 °C; PV + Rot: 0.5 mL L^{-1} PV300 + 1.25 μg L^{-1} roteone; PV + Diu: 0.5 mL L^{-1} PV300 + 5 μg L^{-1} diuron; PV + Dic: 0.5 mL L^{-1} PV300 + 5 μg L^{-1} dicoumarol. Different small letters above the columns represent significant differences among the treatments, which was analyzed by SPSS 20.0 ($P < 0.05$). The error bars represent standard deviation ($n = 3$).

excess ROS accumulation and lipid oxidation. Our findings suggest that PV could be used as a promising algaecide for HAB control, and could also provide a new direction for biomass valorization.

Acknowledgements

This study was supported by the National Natural Science Foundation of China (51378480), NSFC-Shandong Joint Fund for Marine Science Research Centers (U1406403), National Key Basic Research Program of China (2015CB453301).

Appendix A. Supplementary data

Supplementary data associated with this article can be found, in the online version, at http://dx.doi.org/10.1016/j.biortech.2017.09.049.

References

Archambault, M.C., Bricelj, V.M., Grant, J., Anderson, D.M., 2004. Effects of suspended and sedimented clays on juvenile hard clams, *Mercenaria mercenaria*, within the context of harmful algal bloom mitigation. Mar. Biol. 144, 553–565.

Brebu, M., Tamminen, T., Spiridon, I., 2013. Thermal degradation of various lignins by TG-MS/FTIR and Py-GC-MS. J. Anal. Appl. Pyrol. 104, 531–539.

Chen, W., Jia, Y., Li, E., Zhao, S., Zhou, Q., Liu, L., Song, L., 2012. Soil-based treatments of mechanically collected cyanobacterial blooms from lake Taihu: efficiencies and potential risks. Environ. Sci. Technol. 46, 13370–13376.

Chen, W., Song, L., Gan, N., Li, L., 2006. Sorption, degradation and mobility of microcystins in Chinese agriculture soils: risk assessment for groundwater protection. Environ. Pollut. 144, 752–758.

Collard, F.O., Blin, J.L., 2014. A review on pyrolysis of biomass constituents: Mechanisms and composition of the products obtained from the conversion of cellulose, hemicelluloses and lignin. Renewable Sustainable Energy Rev. 38, 594–608.

de Oliveira-Filho, E.C., Lopes, R.M., Paumgartten, F.J.R., 2004. Comparative study on the susceptibility of freshwater species to copper-based pesticides. Chemosphere 56, 369–374.

Demiral, İ., Ayan, E.A., 2011. Pyrolysis of grape bagasse: effect of pyrolysis conditions on the product yields and characterization of the liquid product. Bioresour. Technol. 102, 3946–3951.

Felix, L.C., Folkerts, E.J., He, Y., Goss, G.G., 2017. Poly (acrylic acid)-coated titanium dioxide nanoparticle and ultraviolet light co-exposure has minimal effect on

developing zebrafish (*Danio rerio*). Environ. Sci: Nano 4, 658–669.
Fleming, L.E., Kirkpatrick, B., Backer, L.C., Walsh, C.J., Nierenberg, K., Clark, J., Reich, A., Hollenbeck, J., Benson, J., Cheng, Y.S., 2011. Review of Florida red tide and human health effects. Harmful Algae 10, 224–233.
Gao, Y., Ge, F., Zhang, L., He, Y., Lu, Z., Zhang, Y., Liu, B., Zhou, Q., Wu, Z., 2017. Enhanced toxicity to the cyanobacterium *Microcystis aeruginosa* by low-dosage repeated exposure to the allelochemical N-phenyl-1-naphthylamine. Chemosphere 174, 732–738.
Gu, S., Zheng, H., Xu, Q., Sun, C., Shi, M., Wang, Z., Li, F., 2017. Comparative toxicity of the plasticizer dibutyl phthalate to two freshwater algae. Aquat. Toxicol. 192, 122–130.
Guo, P., Liu, Y., Liu, C., 2015. Effects of chitosan, gallic acid, and algicide on the physiological and biochemical properties of *Microcystis flos-aquae*. Environ. Sci. Pollut. R. 22, 13514–13521.
Hong, Y., Hu, H., Xie, X., Sakoda, A., Sagehashi, M., Li, F., 2009. Gramine-induced growth inhibition, oxidative damage and antioxidant responses in freshwater cyanobacterium *Microcystis aeruginosa*. Aquat. Toxicol. 91, 262–269.
Jančula, D., Maršálek, B., 2011. Critical review of actually available chemical compounds for prevention and management of cyanobacterial blooms. Chemosphere 85, 1415–1422.
Juneja, A., Ceballos, R.M., Murthy, G.S., 2013. Effects of environmental factors and nutrient availability on the biochemical composition of algae for biofuels production: a review. Energies 6, 4607–4638.
Kudela, R.M., Gobler, C.J., 2012. Harmful dinoflagellate blooms caused by *Cochlodinium* sp.: global expansion and ecological strategies facilitating bloom formation. Harmful Algae 14, 71–86.
Kwok, C.T., van de Merwe, J.P., Chiu, J., Wu, R., 2012. Antioxidant responses and lipid peroxidation in gills and hepatopancreas of the mussel *Perna viridis* upon exposure to the red-tide organism *Chattonella marina* and hydrogen peroxide. Harmful Algae 13, 40–46.
Laisk, A., Oja, V., 2013. Thermal phase and excitonic connectivity in fluorescence induction. Photosynth. Res. 117, 431–448.
Lashari, M.S., Ye, Y., Ji, H., Li, L., Kibue, G.W., Lu, H., Zheng, J., Pan, G., 2015. Biochar–manure compost in conjunction with pyroligneous solution alleviated salt stress and improved leaf bioactivity of maize in a saline soil from central China: a 2-year field experiment. J. Sci. Food Agr. 95, 1321–1327.
Li, F., Liang, Z., Zheng, X., Zhao, W., Wu, M., Wang, Z., 2015. Toxicity of nano-TiO_2 on algae and the site of reactive oxygen species production. Aqua. Toxicol. 158, 1–13.
Liang, Y., Zhao, X., Chi, Z., Rover, M., Johnston, P., Brown, R., Jarboe, L., Wen, Z., 2013. Utilization of acetic acid-rich pyrolytic bio-oil by microalga *Chlamydomonas reinhardtii*: reducing bio-oil toxicity and enhancing algal toxicity tolerance. Bioresour. Technol. 133, 500–506.
Liu, N., Wen, F., Li, F., Zheng, X., Liang, Z., Zheng, H., 2016. Inhibitory mechanism of phthalate esters on *Karenia brevis*. Chemosphere 155, 498–508.
Liu, W., Au, D.W.T., Anderson, D.M., Lam, P.K.S., Wu, R.S.S., 2007. Effects of nutrients, salinity, pH and light:dark cycle on the production of reactive oxygen species in the alga *Chattonella marina*. J. Exp. Mar. Biol. Ecol. 346, 76–86.
Liu, W., Li, W., Jiang, H., Yu, H., 2017. Fates of chemical elements in biomass during its pyrolysis. Chem. Rev. 117, 6367–6398.
McFarland, K., Jean, F., Thébault, J., Volety, A.K., 2016. Potential impacts of blooms of the toxic dinoflagellate *Karenia brevis* on the growth, survival and juvenile recruitment of the non-native green mussel *Perna viridis* in southeastern United States. Toxicon 109, 94–102.
Meng, P., Pei, H., Hu, W., Liu, Z., Li, X., Xu, H., 2015. Allelopathic effects of Ailanthus altissima extracts on *Microcystis aeruginosa* growth, physiological changes and microcystins release. Chemosphere 141, 219–226.
Nakai, S., Yamada, S., Hosomi, M., 2005. Anti-cyanobacterial fatty acids released from *Myriophyllum spicatum*. Hydrobiologia 543, 71–78.
Poerschmann, J., Spijkerman, E., Langer, U., 2004. Fatty acid patterns in *Chlamydomonas* sp. as a marker for nutritional regimes and temperature under extremely acidic conditions. Microb. Ecol. 48, 78–89.
Rahmat, B., Pangesti, D., Natawe ijaya, D., Sufyadi, D., 2014. Generation of wood-waste vinegar and its effectiveness as a plant growth regulator and pest insect repellent. BioResources 9, 6350–6360.
Saikia, R., Chutia, R.S., Kataki, R., Pant, K.K., 2015. Perennial grass (*Arundo donax L.*) as a feedstock for thermo-chemical conversion to energy and materials. Bioresour. Technol. 188, 265–272.
Sharma, P., Jha, A.B., Dubey, R.S., Pessarakli, M., 2012. Reactive oxygen species, oxidative damage, and antioxidative defense mechanism in plants under stressful conditions. J. Bot. 2012, 1–26.
Temiz, A., Akbas, S., Panov, D., Terziev, N., Alma, M.H., Parlak, S., Kose, G., 2013. Chemical composition and efficiency of bio-oil obtained from giant cane (*Arundo donax L.*) as a wood preservative. BioResources 8, 2084–2098.
Van Ginkel, S.W., Bidwell, M., Igou, T., Gijon-Felix, R., Salvi, E.J.N.R., De Oliveira, S.H.R., Duarte, L.H.K., Steiner, D., Hu, Z., Johnston, R., Snell, T., Chen, Y., 2016. The prevention of saltwater algal pond contamination using the electron transport chain disruptor-rotenone. Algal Res. 18, 209–212.
Wang, J., Zhu, J., Liu, S., Liu, B., Gao, Y., Wu, Z., 2011. Generation of reactive oxygen species in cyanobacteria and green algae induced by allelochemicals of submerged macrophytes. Chemosphere 85, 977–982.
Wang, Z., Cao, J., Wang, J., 2009. Pyrolytic characteristics of pine wood in a slowly heating and gas sweeping fixed-bed reactor. J. Anal. Appl. Pyrol. 84, 179–184.
WHOI, 2016. Distribution of HABs in World. Woods Hole Oceanographic Institution, USA.
Wu, Q., Zhang, S., Hou, B., Zheng, H., Deng, W., Liu, D., Tang, W., 2015. Study on the preparation of wood vinegar from biomass residues by carbonization process. Bioresour. Technol. 179, 98–103.
Yang, C., Liu, S., Zhou, S., Wu, H., Yu, J., Xia, C., 2011. Allelochemical ethyl 2-methyl acetoacetate (EMA) induces oxidative damage and antioxidant responses in *Phaeodactylum tricornutum*. Pestic. Biochem. Phys. 100, 93–103.
Yang, J., Yang, C., Liang, M., Gao, Z., Wu, Y., Chuang, L., 2016. Chemical composition, antioxidant, and antibacterial activity of wood vinegar from *Litchi chinensis*. Molecules 21, 1150–1159.
Zheng, H., Wang, X., Chen, L., Wang, Z., Xia, Y., Zhang, Y., Wang, H., Luo, X., Xing, B., 2017. Enhanced growth of halophyte plants in biochar-amended coastal soil: roles of nutrient availability and rhizosphere microbial modulation. Plant, Cell Environ. http://dx.doi.org/10.1111/pce.12944.
Zheng, H., Wang, X., Luo, X., Wang, Z., Xing, B., 2018. Biochar-induced negative carbon mineralization priming effects in a coastal wetland soil: Roles of soil aggregation and microbial modulation. Sci. Total Environ. 610–611, 951–960.
Zheng, H., Wang, Z., Deng, X., Zhao, J., Luo, Y., Novak, J., Herbert, S., Xing, B., 2013. Characteristics and nutrient values of biochars produced from giant reed at different temperatures. Bioresour. Technol. 130, 463–471.
Zhou, L., Zheng, T., Chen, X., Wang, X., Chen, S., Tian, Y., Hong, H., 2008. The inhibitory effects of garlic (*Allium sativum*) and diallyl trisulfide on *Alexandrium tamarense* and other harmful algal species. J. Appl. Phycol. 20, 349–358.